Available online at www.sciencedirect.com

SciVerse ScienceDirect

Ceramics International 38 (2012) 3851–3856

CERAMICS INTERNATIONAL

www.elsevier.com/locate/ceramint

Magnesia stabilized zirconia doped with boron, ceria and gadolinia

A. Aytimur [a], I. Uslu [a,*], S. Koçyiğit [a], F. Özcan [b]

[a] Gazi University, Gazi Faculty of Education, Teknikokullar, Ankara 06500, Turkey
[b] Selçuk University, Faculty of Science, Selçuklu, Konya 42075, Turkey

Received 27 December 2011; received in revised form 11 January 2012; accepted 12 January 2012
Available online 21 January 2012

Abstract

In this study, magnesia stabilized zirconia based nanocrystalline ceramics were produced through a polymer precursor route using gadolinium and boron. The powders were characterized during the various steps by structural and morphological techniques (FT-IR, XRD, and SEM). XRD results proved that a tetragonal phase is predominant for all samples with varying magnesium contents and no monoclinic zirconia solid solution appears. The crystallite sizes of the samples were calculated using Scherrer equation. The smallest crystallite size was obtained for the sample containing Zr/Mg/Ce/Gd/B ratio of 82/0/10/8/0. The lattice parameters were calculated for cubic, tetragonal, hexagonal, and orthorhombic structures. SEM results show all the samples have spherical grains. The average grain diameters were calculated for all the samples. The smallest average grain diameter was obtained for the sample containing Zr/Mg/Ce/Gd/B ratio of 82/0/10/8/0.

Keywords: B. Nanocomposites; D. CeO_2; D. MgO; D. ZrO_2; Polymer precursor

1. Introduction

Zirconia (ZrO_2) is one of the most promising materials for a new generation of ceramics and catalysts [1,2].

Zirconia stabilized by metal oxide has shown an outstanding structural stability which includes a very good resistance to corrosion under heat, aqueous solutions, high thermal conductivity, and irradiation stability. Because of these properties, stabilized ZrO_2 elements have been applied as catalysts in high degree alkane isomerizations, as electrolytes in solid oxide fuel cells (SOFC), as oxygen sensors in air pollution control or production of inert matrix fuel [3–5].

Zirconia can be stabilized down to room temperature by being doped with MgO [6]. Aside from a suitable amount of magnesia, rare earths may also be introduced to zirconia in order to increase the high oxygen mobility and oxygen storage capacity (OSC) of the ceramic for a majority of the current applications. Doping magnesia stabilized zirconia with ceria [7] and gadolinia [8] not only allows ensuring material stability but also was recently investigated with the intention of improving oxygen mobility of the final ceramic material, especially in regards to SOFC applications.

Numerous studies made in recent years on advanced ceramic material applications demonstrated that boric oxide (B_2O_3) is an effective sintering aid [9] and an excellent network former [10]. The effect of the addition of H_3BO_3 on the sintering of ZnO was investigated by Kushnirenko et al. [11], who came to the conclusion that the addition of boric acid resulted in the rise of grain size, the increase of grain conductivity, the quenching of defect-related luminescence, and the enhancement of exciton emission. Misirli et al. [12] researched what the effect of an addition of B_2O_3 on the sintering of Al_2O_3 was, and they found that the porosity of the materials, which were produced using a spray-drying technique, could be controlled by the addition of levels of B_2O_3. By giving the material a good strength, this porous structure made it a potential candidate for being used in ceramic filters and for ceramic–metal composite preforms [13].

The fabrication and characterization of the calcined partially stabilized zirconia (ZrO_2) with magnesia (MgO) using polymer derived ceramic technique is described in this paper. The calcined ceramic powders mentioned should be sintered at high temperatures (>1400 °C) in air or in a reducing gas atmosphere in order to produce dense and more thermodynamically stable solid phases with the desired pore structures.

* Corresponding author. Tel.: +90 312 202 8017; fax: +90 312 202 8041.
E-mail address: uslui_1955@yahoo.com (I. Uslu).

0272-8842/$36.00
doi:10.1016/j.ceramint.2012.01.035

This novel route includes mixing the pre-ceramic precursors of zirconium, magnesium and gadolinium acetates, and boric acid with the appropriate concentration of the polyvinyl alcohol (PVA) solution to prepare a hybrid polymer solution. PVA was used as the polymerization agent due to its comparatively long molecular chain [14].

2. Materials and methods

In the experiments, the PVA (average molecular weight of 85,000–124,000, Sigma–Aldrich), the cerium(III) acetate (Sigma–Aldrich), the gadolinium(III) acetate (Sigma–Aldrich), the zirconium acetate (solution in dilute acetic acid, Sigma–Aldrich), the magnesium acetate (Merck), and boric acid (Merck) were used and ultrapure deionized water was used as a solvent.

The experiments were carried out in three major steps: (i) the preparation of the metal acetate composite precursor hybrid polymeric (PVA) solution, (ii) heating the prepared polymeric solution to obtain hydrogel solution containing metal acetate in the furnace at 80 °C, (iii) the calcination or the chemical conversion of the hydrogel solution into the desired ceramic nanopowder at an elevated temperature, with concomitant removal of all the hybrid PVA polymer solutions from the precursor at 850 °C. The heating and cooling rates were fixed at 8 °C/min.

The aqueous PVA solution (10%) was first prepared by dissolving the PVA powder in ultra pure distilled water and heating it to 80 °C, stirring it for 3 h, and then, cooling it down to room temperature while continuously stirring it for 2 more hours. In the experiments, five hybrid polymer solutions were separately prepared and compared in order to see the effect of Mg, Ce, Gd and B on the calcination behavior and to provide further opportunity to explore possible compositional dependence of the micro-structure.

For each composition, proper proportions of metal acetate solutions were added drop by drop to a 20 g aqueous PVA at 60 °C (see Table 1 for details) and each hybrid polymer solutions were stirred vigorously using a magnetic stirring bar for 3 h at this temperature.

As a final product, viscous gels of the boron doped PVA/Zr–Mg–Ce–Gd acetate hybrid polymer solutions were prepared. The hybrid polymer solutions dried at room temperature and finally were transferred into ceramic crucibles, and then, calcined in air atmosphere at 850 °C for 2 h at a heating rate of 8 °C/min. Resulting oxide ceramic composites obtained from solutions 1–5, named as IMF 1–5, were ground into powder using a mortar.

Table 1
Metal concentrations in the synthesized ceramics % (wt/wt).

Solution #	% Zr	% Mg	% Ce	% Gd	% B
1	82.0	0.0	10.0	8.0	0.0
2	65.0	10.0	13.0	10.0	2.0
3	49.0	20.0	16.0	12.0	3.0
4	33.0	30.0	19.0	14.0	4.0
5	0.0	57.0	22.0	16.0	5.0

The pH and conductivity of the solutions were measured by using Wissenschaftlich-Technische-Werkstätten WTW and 315i/SET apparatus. The viscosity values of the hybrid polymer solutions were measured with AND SV-10 viscometer. The surface tension values of the complex hybrid polymer solutions were measured by using KRUSS model manual measuring system. Fourier Transformations Infrared Spectroscopy (FT-IR) with ATR module results were obtained using Thermo Nicolette 6700 spectrophotometer. Composite morphology was observed by scanning electron microscopy technique using JEOL JSM 6060 on samples sputtered with gold and observed at an accelerating voltage of 10 kV. Particle diameters were measured by image processing software, ImageJ (Image Pro-Express, Version 5.0.1.26, Media Cybernetics Inc.) which is a public domain Java image processing program [15]. The crystal structures of the calcined powders were investigated by means of X-ray diffraction using XRD Bruker AXS D8 Advance diffractometer with Vario1 Johansson focusing monochromator Cu Kα1 radiation.

3. Results and discussion

The pH, viscosity, conductivity and surface tension of the hybrid polymer solutions were measured and obtained values are given in Table 2. The increase in amounts of Mg, Ce, Gd, and B increased the pH, viscosity, conductivity and surface tension of solutions.

FT-IR spectroscopy was performed to gain more information about the structures of IMF 1–5 solutions and calcined powders. The FT-IR spectra of the IMF 1–5 solutions are given in Fig. 1(a–e). The large bands observed between 3600 and 3200 cm^{-1} are linked to the stretching O–H vibration. The vibrational band observed between 3000 and 2840 cm^{-1} refers to the stretching C–H vibration of alkyl groups. The band observed at 1706 and 1640 cm^{-1} are attributed to C=O stretching and C–O stretching of PVA, respectively. The band observed 1391 cm^{-1} is attributed to O–H vibration. The band observed at 1273 cm^{-1} refers to C–O stretching. The band observed at 1016 cm^{-1} refers to the characteristic vibration of acetic acid (CH_3COOH). The band at 615 cm indicates the out of plane vibrations of O–H in PVA.

Fig. 2(a–e) is the FT-IR spectra of nanocrystalline powder samples IMF 1–5.

As shown in Fig. 2, neither the broad band at 3600–3200 cm^{-1} nor the band at 3000–2840 cm^{-1} was observed for calcined IMF 1–5 nanocrystalline powder samples. As mentioned before, these bands are attributed to the stretching O–H vibration and the stretching C–H vibration of alkyl groups, respectively. The absence of these bands indicated the absence of both water and carbon content in the nanocrystalline powder samples. The bands, which were observed at 1292 and 1197 cm^{-1}, are thought to arise due to magnesia, ceria or gadolinia. Moreover, intensities of these bands increased due to the increase in amounts of magnesium, cerium and gadolinium contents. The band observed at 720 cm^{-1} assigned to the bending vibrations of various borate segments [16].

Table 2
Physical properties of the boron doped PVA/Zr–Mg–Ce—Gd acetate hybrid polymer solution.

Solution #	pH	Viscosity (mPa s)	Conductivity (mS cm^{-1})	Surface tension (mN m^{-1})
1	2.82	72.6	2.080	46
2	3.30	98.3	6.360	49
3	3.49	114.0	9.690	51
4	3.60	153.0	12.290	52
5	3.82	209.0	16.770	54

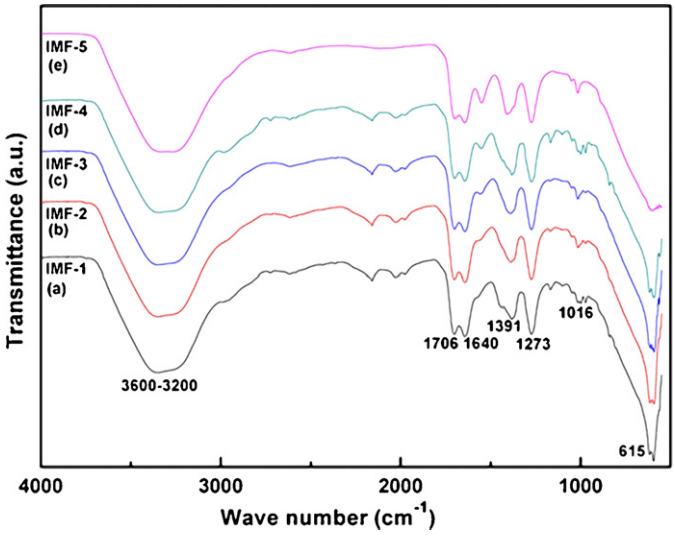

Fig. 1. FT-IR spectra of: (a) IMF-1, (b) IMF-2, (c) IMF-3, (d) IMF-4, and (e) IMF-5 solutions.

Figs. 3 and 4 show typical XRD spectrum of the magnesia stabilized zirconia based nanocrystalline ceramics doped with gadolinium and boron. XRD patterns given in Fig. 3(a and b) exhibits the ZrO_2 crystal structure of the IMF-1 and the IMF-2 samples. The IMF-1 sample contains no MgO and B_2O_3 with small amounts of CeO_2 and Gd_2O_3. The IMF-2 sample contains small amount of MgO and B_2O_3 with increased amount CeO_2 and Gd_2O_3 with respect to the IMF-1 sample. A decrease in the brittleness occurs in ZrO_2 crystal structure when a small amount of MgO is added to the composite [17]. As a result, one phase mixture of stabilized tetragonal $Zr_{1-x}Ce_xO_2$ structures was identified for both of the samples with five reflection peaks, appeared at 2θ values of 30.02° (1 0 1), 34.71° (0 0 2), 49.99° (1 1 2), 59.73° (1 0 3) and 62.31° (2 0 2), according to JCPDS-International Center for Diffraction Data (PDF # 01-088-2397). These peaks are in very good agreement with the JPDS diffraction data. To avoid the cracking problem due to the volume increase during the phase change it is desirable that zirconia keeps in tetragonal phase in relatively wide range of temperature [18]. As seen from Figs. 3 and 4, IMF 1–4 nanocrystalline powder samples have one phase mixture of stabilized tetragonal $Zr_{1-x}Ce_xO_2$ structures.

With higher Mg composition (for the IMF-3 and the IMF-4 samples), as expected intensity of ZrO_2 peaks at 30.02°, 34.71°, 49.99°, 59.73°, 62.31° is decreased and minor peaks are disappeared. The addition of Mg into $ZrCeO_2$ is not interfere main tetragonal structure of $ZrCeO_2$. These results suggest that magnesia was dispersed well within ceramic structure.

The cubic structure continues to build in with increasing MgO, CeO_2, Gd_2O_3, and B_2O_3 contents due to the absence of zirconium content (for the IMF-5). The ceramics were found to consist of not a single phase, but rather multiphase (cubic, tetragonal, hexagonal, and orthorhombic structures) materials according to JCPDS-International Center for Diffraction Data (PDF # 00-005-0648, 00-011-0608, 01-071-1176, and 00-013-0483) [19].

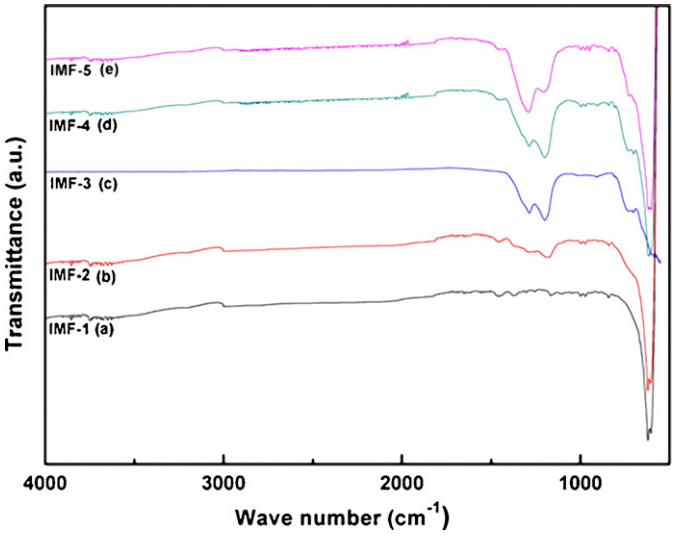

Fig. 2. FT-IR spectra of the nanocrystalline: (a) IMF-1, (b) IMF-2, (c) IMF-3, (d) IMF-4, and (e) IMF-5 powder samples.

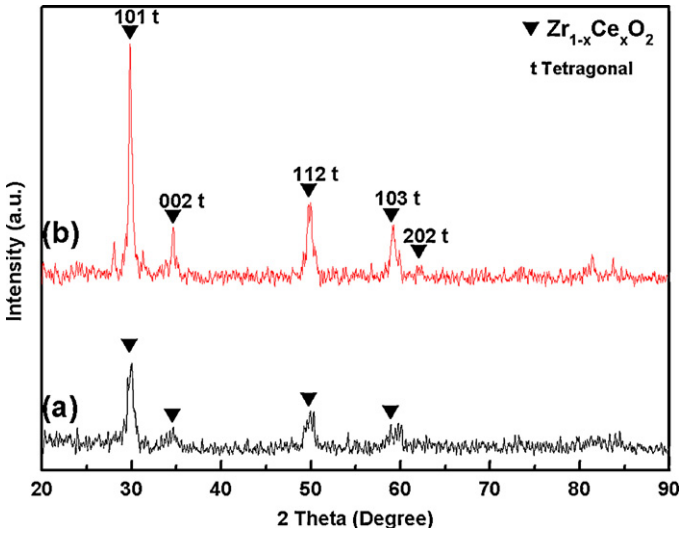

Fig. 3. X-ray diffraction patterns of the nanocrystalline: (a) IMF-1, and (b) IMF-2 powder samples.

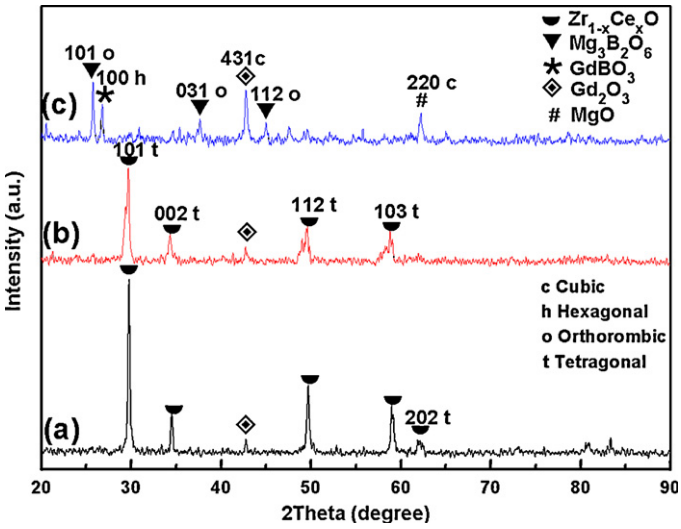

Fig. 4. X-ray diffraction patterns of the nanocrystalline: (a) IMF-3, (b) IMF-4, and (c) IMF-5 powder samples.

The crystallite sizes (D) were calculated based upon on the (1 0 1) diffraction peak's broadening in the XRD pattern using the Scherrer equation [20–24]:

$$D_{hkl} = \frac{k\lambda}{\beta_{hkl}\cos\theta} \tag{1}$$

where $D_{h\,k\,l}$ is the average dimension of the crystallites, $k = 0.9$, λ is the wavelength of the X-ray radiation (0.15405 nm), θ is the Bragg angle for the crystal planes $\{h\,k\,l\}$, and $\beta_{h\,k\,l}$ is the broadening (full-width at half-maximum (FWHM)) of the peak. The crystallite sizes were calculated as 10.8 nm (1.08×10^{-8} m), 16.9 nm (1.69×10^{-8} m), 20.4 nm (2.04×10^{-8} m), 13.5 nm (1.35×10^{-8} m), and 18.8 nm (1.88×10^{-8} m) for IMF-1, IMF-2, IMF-3, IMF-4, and IMF-5 samples, respectively.

The lattice parameters of the composite samples were determined by comparing the peak positions (2θ) of the XRD patterns using the below relations for cubic structures (Eq. (2)), tetragonal structures (Eq. (3)), hexagonal structures (Eq. (4)), and orthorhombic structures (Eq. (5)) [25]:

$$\frac{1}{d^2} = \frac{h^2 + k^2 + l^2}{a^2} \tag{2}$$

$$\frac{1}{d^2} = \frac{h^2 + k^2}{a^2} + \frac{l^2}{c^2} \tag{3}$$

$$\frac{1}{d^2} = \frac{4}{3}\left(\frac{h^2 + hk + k^2}{a^2}\right) + \frac{l^2}{c^2} \tag{4}$$

$$\frac{1}{d^2} = \frac{h^2}{a^2} + \frac{k^2}{b^2} + \frac{l^2}{c^2} \tag{5}$$

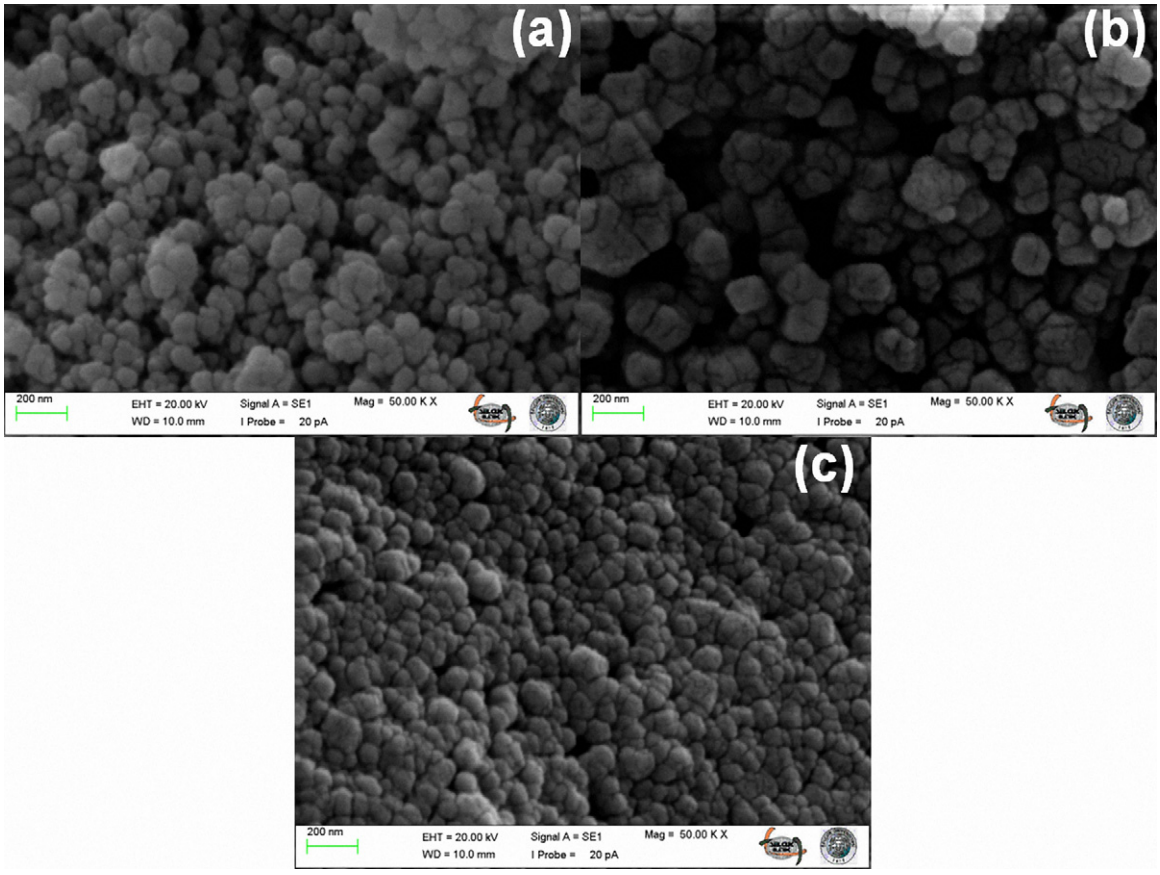

Fig. 5. SEM micrographs of the nanocrystalline: (a) IMF-1, (b) IMF-4, and (c) IMF-5 powder samples.

According to calculated results, the smallest lattice constants for tetragonal structure, a and c, were obtained for the IMF-1 sample. The calculated structural lattice parameters, a and c, for the IMF-1 sample of the (1 0 3) reflection were 3.5775 Å and 5.1467 Å, respectively. For samples of higher Mg content (the IMF 3,4) XRD measurement shows that the cubic structure continues to build in with increasing MgO. The lattice constants for cubic structure, a, were calculated as 10.7548 Å, 10.7836 Å, and 10.7692 Å for the IMF-3, the IMF-4, and the IMF-5 samples of the (4 3 1) reflection, respectively. The lattice parameters for orthorhombic structure, a–c, were calculated for the IMF-5 sample has no zirconia.

SEM images of the magnesia stabilized zirconia based nanocrystalline ceramics doped with gadolinium and boron nanocrystalline powder samples calcined at 850 °C are taken at 5×10^4 magnitude and they are shown in Fig. 5. All the particles are almost spherical in shape grains of regular form, smaller than powders produced by conventional powder mixing, pressing and sintering technique [26].

According to the grain size diameter distribution of all the IMF samples, obtained crystalline samples are at nanoscale in size and distribution of the spherical grain particles are in the range around 50–180 nm. Grain diameters of the IMF-1 samples range from 50 nm to 80 nm. Grain diameters of the IMF-2 samples range from 90 nm to 140 nm. Grain distribution with a range from 110 nm to 180 nm is obtained for the IMF-3 sample. Grain diameters of the IMF-4 range from 120 nm to 180 nm. Grain diameters of the IMF-5 crystalline samples range from 50 nm to 110 nm. The average grain diameters for all samples were calculated as 66 nm, 111 nm, 141 nm, 146 nm, and 80 nm for IMF-1, IMF-2, IMF-3, IMF-4, and IMF-5 nanocrystalline ceramic samples, respectively.

4. Conclusions

Magnesia stabilized zirconia using gadolinium and boron was obtained by polymer precursor route. The crystalline structures were characterized by FT-IR, XRD and SEM. The results demonstrated that addition of magnesia stabilized zirconia using gadolinium and boron providing nanosized particles. From results presented in this paper, Mg content of magnesium acetate to produce Mg stabilized zirconia consisting of nanosized crystallite grains and cross-linking boundaries between grains after heat treatment at 850 °C could be a very promising starting material for ceramic IMF fabrication. XRD results proved that a tetragonal phase is predominant for all samples with varying magnesium contents and no monoclinic zirconia solid solution appears. Calculated crystallite sizes (D) were 10.8 nm (1.08×10^{-8} m), 16.9 nm (1.69×10^{-8} m), 20.4 nm (2.04×10^{-8} m), 13.5 nm (1.35×10^{-8} m), and 18.8 nm (1.88×10^{-8} m) for IMF-1, IMF-2, IMF-3, IMF-4, and IMF-5 samples, respectively. SEM results show all the samples have spherical grains. Moreover, the average grain diameters were calculated as 66 nm, 111 nm, 141 nm, 146 nm, and 80 nm for IMF-1, IMF-2, IMF-3, IMF-4, and IMF-5 nanocrystalline ceramic samples, respectively. Interpretation of grain diameter calculation and crystallite size calculation shows that IMF-4 nanoparticles were agglomerated. Moreover, all the IMF samples are at nanoscale.

References

[1] Y.W. Li, D.H. He, Y.B. Yuan, Z.X. Cheng, Q.M. Zhu, Influence of acidic and basic properties of ZrO_2 based catalysts on isosynthesis, Fuel 81 (2002) 1611.

[2] A. Clearfield, G.P.D. Serrette, A.H. Khazisyed, Nature of hydrous zirconia and sulfated hydrous zirconia, Catal. Today 20 (1994) 295.

[3] A. Imaura, N. Touran, R.C. Ewing, MgO–pyrochlore composite as an inert matrix fuel: neutronic and thermal characteristics, J. Nucl. Mater. 389 (2009) 341.

[4] S. Kikuyama, I. Matsukuma, R. Kikuchi, K. Sasaki, K. Eguchi, Effect of preparation methods on NO_x removal ability by sorption in Pt–ZrO_2–Al_2O_3, Appl. Catal. A: Gen. 219 (2001) 107.

[5] L.M. Gandia, M.A. Vicent, A. Gil, Complete oxidation of acetone over manganese oxide catalysts supported on alumina- and zirconia-pillared clays, Appl. Catal. B: Environ. 38 (2002) 295.

[6] N. Navruz, Application of the infinitesimal deformation approach to the tetragonal-to-monoclinic transformation in MgO-partially-stabilized zirconia, Philos. Mag. Lett. 84 (2004) 15.

[7] J. Mikulova, S. Rossignol, F. Gerard, D. Mesnard, C. Kappenstein, D. Duprez, Properties of cerium–zirconium mixed oxides partially substituted by neodymium: comparison with Zr–Ce–Pr–O ternary oxides, J. Solid State Chem. 179 (2006) 2511.

[8] E.N.S. Muccillo, R.A. Rocha, R. Muccillo, Preparation of Gd_2O_3-doped ZrO_2 by polymeric precursor techniques, Mater. Lett. 53 (2002) 353.

[9] R.A. Smith, Basic geology and chemistry of borate, Am. Ceram. Soc. Bull. 81 (2002) 61.

[10] E.E. Horopanitis, G. Perentzis, A. Beck, L. Guczi, G. Peto, L. Papadimitriou, Correlation between structural and electrical properties of heavily lithiated boron oxide solid electrolytes, J. Non-Cryst. Solids 354 (2008) 374.

[11] V.I. Kushnirenko, I.V. Markevich, A.V. Rusavsky, Influence of boric acid as a flux on the properties of ZnO ceramics, Radiat. Meas. 45 (2010) 468.

[12] Z. Misirli, H. Erkalfa, O.T. Ozkan, Effect of B_2O_3 addition on the sintering of α-Al_2O_3, Ceram. Int. 22 (1996) 33.

[13] I. Uslu, M.K. Ozturk, M.L. Aksu, F. Gokmese, Fabrication and characterization of boron doped Ni/Zn acetate nanofibers, Synth. React. Inorg. Met. 39 (2009) 199.

[14] S.K. Saha, A. Pathak, P. Pramanik, Low-temperature preparation of fine particles of mixed-oxide systems, J. Mater. Sci. Lett. 14 (1995) 35.

[15] http://rsbweb.nih.gov/ij/docs/intro.html (last accessed 24.12.11).

[16] L. Griguta, I. Ardelean, Structural investigation of Gd_2O_3–B_2O_3–Li_2O glasses by FT-IR and Raman spectroscopies, J. Optoelectron. Adv. Mater. 10 (2008) 256.

[17] D. Michel, L. Mazerolles, M. Perez, Y. Jorba, Fracture of metastable tetragonal zirconia crystals, J. Mater. Sci. 18 (1983) 2618.

[18] B. Robertz, A. Rulmont, B. Gilbert, R. Cloots, M. Ausloos, N. Leroy, Inhibition of the macrocrack formation in zirconia substrates by barium zirconate formation, Mater. Lett. 41 (1999) 273.

[19] Y. Nagai, T. Yamamoto, T. Tanaka, S. Yoshida, T. Nonaka, T. Okamoto, A. Suda, M. Sugiura, X-ray absorption fine structure analysis of local structure of CeO_2–ZrO_2 mixed oxides with the same composition ratio (Ce/Zr = 1), Catal. Today 74 (2002) 225.

[20] B. Karunagaran, R.T.R. Kumar, D. Mangalaraj, S.K. Narayandass, G.M. Rao, Influence of thermal annealing on the composition and structural parameters of DC magnetron sputtered titanium dioxide thin films, Cryst. Res. Technol. 37 (2002) 1285.

[21] P.H. Klug, L.E. Alexander, X-ray Diffraction Procedures for Polycrystalline and Amorphous Materials, Wiley, New York, 1974.

[22] N.S. Prasad, K.B.R. Varma, Nanocrystallization of $SrBi_2Nb_2O_9$ from glasses in the system $Li_2B_4O_7$–SrO–Bi_2O_3–Nb_2O_5, Mater. Sci. Eng. B: Solid 90 (2002) 246.

[23] E. Alvarado, L.M. Torres-Martinez, A.F. Fuentes, P. Quintana, Preparation and characterization of MgO powders obtained from different magnesium salts and the mineral dolomite, Polyhedron 19 (2000) 2345.
[24] Y. Ding, G.T. Zhang, H. Wu, B. Hai, L.B. Wang, Y.T. Qian, Nanoscale magnesium hydroxide and magnesium oxide powders: control over size, shape, and structure via hydrothermal synthesis, Chem. Mater. 13 (2001) 435.
[25] C. Suryanarayana, M.G. Norton, X-ray Diffraction a Practical Approach, Plenum Press, New York, 1998.
[26] N. Kamel, H. Ait-Amar, M. Taouinet, C. Benazzouz, Z. Kamel, H. Fodil-Cherif, S. Telmoune, R. Slimani, A. Zahri, D. Sahel, Comparative study of simulated zirconia inert matrix fuel stabilized with yttrium, lanthanum or praseodymium: synthesis and leaching tests, Prog. Nucl. Energy 48 (2006) 70.